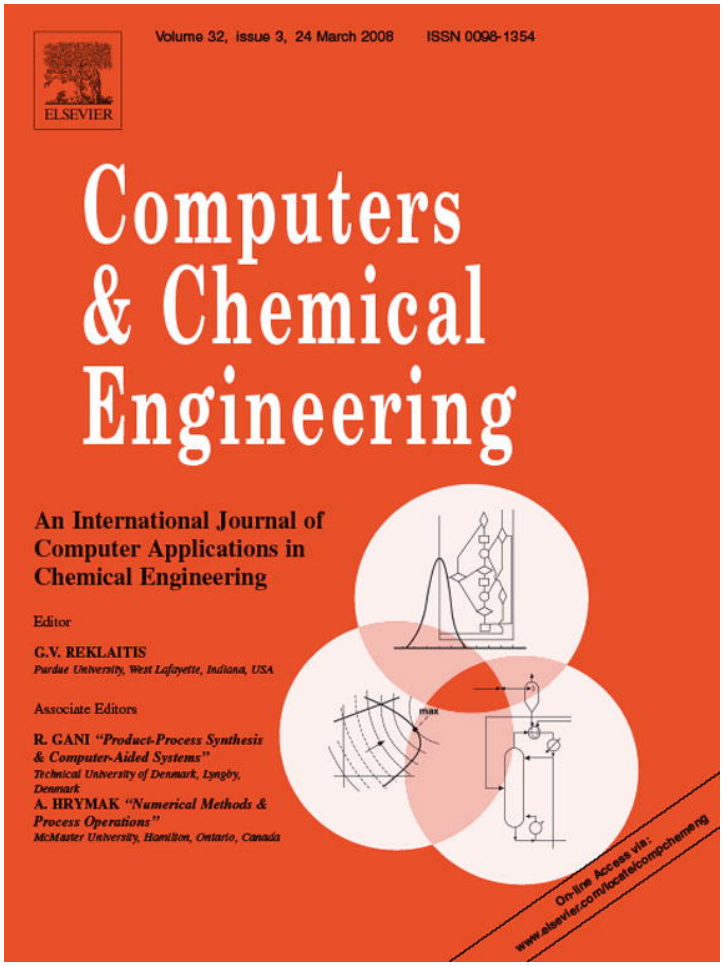

Available online at www.sciencedirect.com
ScienceDirect
Computers and Chemical Engineering 32 (2008) 396–408
Computers & Chemical Engineering
www.elsevier.com/locate/compchemeng

Modeling and optimization of a high-pressure ethylene polymerization reactor using gPROMS

Mariano Asteasuain, Adriana Brandolin *

Planta Piloto de Ingeniería Química (Universidad Nacional del Sur-CONICET), Camino La Carrindanga km 7, C.C. 717, 8000 Bahía Blanca, Argentina

Received 24 October 2006; received in revised form 19 February 2007; accepted 22 February 2007
Available online 27 February 2007

Abstract

A gPROMS implementation of a comprehensive steady-state model of the high-pressure polymerization of ethylene in a tubular reactor is presented. Model outputs along the reactor length include the complete molecular weight distribution and branching indexes, as well as monomer conversion, average molecular weights, reactants' compositions, and reactor temperature and pressure. A detailed calculation of physical and transport properties, such as the reaction mixture density, heat-transfer capacity, viscosity and global heat-transfer coefficient is also included. The reactor model is included in an optimization framework that is used to determine the best operating conditions for producing a polymer with tailor-made molecular structure in terms of the complete molecular weight distribution, branching and polydispersity.

Keywords: Polyethylene; Polymerization; Molecular weight distribution; Mathematical models; Optimization; Tubular reactor; gPROMS; FORTRAN

1. Introduction

High-pressure polymerization of ethylene in tubular reactors is a widely used process to produce low density polyethylene (LDPE), a commodity polymer with a very important market. This process is carried out in jacketed tubes under rigorous operating conditions. The main feed to the reactor usually consists of ethylene and inerts, transfer agents to control the molecular weight, and eventually oxygen to start the reaction. Most of the polymerization reaction, however, is initiated by peroxides that are fed to the reactor through lateral injections. Monomer and/or transfer agents can also be fed through side feedings. The polymerization takes place in short reaction zones following the peroxides injections, with high heat generation. The rest of the reactor is mainly used as a heat exchanger, in order to reach appropriate temperatures for peroxides addition or for downstream units. The control of the reaction mixture temperature is achieved by circulating water through the tube jackets. Typical operating conditions involve temperatures ranging from 50 ° C at the reactor entrance to almost 335 ° C at the peaks, pressures of 2000 bar or more, and axial velocities of around 10–12 m/s. Evidently, the reactor configuration is very complex. The economic importance of the process and the necessity of counting with a tool for studying safely and economically the influence of the different design and operating variables, have motivated the development of several mathematical models for the process since the 1960s, as reviewed elsewhere (Kim & Iedema, 2004; Zabisky, Chan, Gloor, & Hamielec, 1992). It should be mentioned that detailed, rigorous models validated against data from actual industrial reactors have been presented (Brandolin, Lacunza, Ugrin, & Capiati, 1996; Kiparissides, Verros, Kalfas, Koutoudi, & Kantzia, 1993; Lacunza, Ugrin, Brandolin, & Capiati, 1998). However, simplifications with respect to actual reactor configurations and operating conditions, such as constant jacket temperature, pressure and/or global heat transfer coefficient have sometimes been employed, specially in those models used for optimization purposes (Asteasuain, Ugrin, Lacunza, & Brandolin, 2001).

Most of the tubular reactor models available in the literature deal with the prediction of average values of distributed properties, such as branching indexes or average molecular weights. In this work, we are particularly interested in the modeling of the full distribution of molecular weights and the branching indexes.

* Corresponding author. Tel.: +54 291 4861700; fax: +54 291 4861600.
E-mail addresses: masteasuain@plapiqui.edu.ar (M. Asteasuain), abrandolin@plapiqui.edu.ar (A. Brandolin).

0098-1354/$ – see front matter © 2007 Elsevier Ltd. All rights reserved.
doi:10.1016/j.compchemeng.2007.02.011

It is well known that molecular weight distribution (MWD) is responsible for several end-use and processing properties of polymers, as discussed in Wells and Ray (2005). Besides, long and short chain branches also play a very important role in these polymer properties. Long chain branching has a strong impact on the rheological behavior of the polymer. It affects the polymer melt properties (e.g. extensional viscosity, shear viscosity and elasticity) and the polymer solid state properties (e.g. orientation effects and stressed induced crystallization) (Pladis & Kiparissides, 1998). In its turn, short chain branching is responsible for the low density of the polymer. Therefore, long and short branching frequencies are also key molecular parameters in defining polymer quality. It should be noted that the MWD and branches are not independent molecular properties. Therefore, if the process is modified taking only one of these properties into account, the others may take undesired values. A mathematical model of a LDPE tubular reactor able to predict the full MWD and branching index can be used as a powerful optimization tool. For instance, it could be applied in finding the operating conditions for producing a polymer with specific molecular architecture. However, this task represents a challenge due to the mathematical complexity involved, particularly in the case of the complete MWD. There are few models reported in the literature capable of calculating this molecular property. For instance, Kim and Iedema (2004) used the PREDICI® software package, which uses a discrete Galerkin method to compute the full MWD, to model the polyethylene MWD in a tubular reactor. A single comparison between an experimental and the corresponding modeled MWD was presented. The authors analyzed the effects of different scission mechanisms, lineal, topological and mechanical scission, on the MWD. They also performed sensitivity studies on scission kinetics and the effect of chain transfer agent (CTA). They simulated alternative CTA injection strategies, showing that downstream positions could lead to broad and even bimodal distributions, which is rarely observed in usual operation of industrial tubular reactors. They concluded that tubular reactors allowed manipulating the MWD to a great extent. Schmidt, Busch, Lilge, and Wulkow (2005) also employed PREDICI® to model a two-dimensional distribution, in molecular weight as well as in branching frequency. Simulation results were compared with experimental data. They considered the effect of residence time distribution by considering a two compartment model. The authors mention that their work is a first step in a process aiming to design application properties of the polymer. Subsequent steps would be to correlate the molecular structure (branching, MWD) with the application properties, and then reverse the sequence to find the operating conditions that would lead to desired product quality. None of these works attempted to tailor the complete MWD and branches.

In this work, we implement a model of the high-pressure ethylene polymerization in a tubular reactor that deals not only with the complete MWD but also the branching indexes as function of the reactor axial distance. A previous, rigorous model of the reactor (Brandolin et al., 1996), implemented in FORTRAN code, was first extended to calculate the complete MWD (Asteasuain & Brandolin, 2006). The new model was implemented in gPROMS (Process Systems Enterprise, Ltd.). This software was selected because the mathematical model can be easily included in its advanced optimization algorithms. Now the model is further updated to incorporate the prediction of the number average of short and long branches, as well as vinyl and vinylidene groups content. Efficient modeling of lateral feedings, which involve discontinuities in some of the differential variables, is developed. The MWD is determined by means of the probability generating function (pgf) technique developed by the authors (Asteasuain, Brandolin, & Sarmoria, 2002; Asteasuain, Sarmoria, & Brandolin, 2002). This technique uses no prior assumption on the type of distribution, so that it is possible to use it to model any distribution shape. Besides, it is very easy to include the pgf equations in the process model, in spite of the complex kinetic mechanism and reactor configuration. In this work, we provide complete details about the implementation of the pgf technique in gPROMS, including the corresponding model equations and inversion algorithm. The capability of gPROMS to perform the mathematical computations efficiently is determined. Model validation for the complete MWD prediction is performed against experimental data by comparing experimental values of the average molecular weights with those calculated from the predicted MWDs. Since our former FORTRAN model had been thoroughly tested against experimental data, the gPROMS model was compared with the FORTRAN model for those variables predicted by both of them, like the average molecular weights, conversion and branches. The rigorous model of the polymerization reactor presented here is included in an optimization framework that is used to determine the best operating conditions for producing a polymer with tailored-made MWD and branches. Application examples are presented to show the potential benefits of this tool. They involve maximization of reactor productivity at a specific polymer quality in terms of the whole MWD and branches, and obtaining bimodal distributions with constrained polydispersity. An efficient approach is developed for seeking for a bimodal distribution using information of few points of the MWD, taking advantages of the pgf properties.

2. Polymerization reactor model

The mathematical model of the reactor is constructed on the basis of previous works by the authors (Asteasuain, Pereda, Lacunza, Ugrin, & Brandolin, 2001; Brandolin et al., 1996; Lacunza et al., 1998). Brandolin et al. (1996) and Lacunza et al. (1998) developed an exhaustive mathematical model for the high pressure polymerization of ethylene in tubular reactors, considering configurations similar to those encountered in industry. For instance, multiple injections of monomer, mixtures of initiators and transfer agents were taken into account, as well as realistic flux configurations. Besides, a detailed calculation of physical and transport properties, such as the reaction mixture density, heat-transfer capacity, viscosity, global heat-transfer coefficient, etc., along the axial distance was included. The mathematical model was validated against several data sets from an actual industrial reactor.

Asteasuain, Pereda, et al. (2001) revised the mathematical model used in Brandolin et al. (1996) in order to develop a reduced model suitable for faster parameter adjustment. They obtained a subset of the kinetic steps that is crucial to the description of the polymerization process. They found that initiator and transfer agent mixtures could be treated as single fictitious species. They also proved that constant jacket temperature at each reactor zone was a reasonable assumption for the current operating conditions of the reactor. This resulted in a model that could be adjusted rapidly to predict the behavior of a specific industrial reactor. This analysis was also checked against data from the same industrial reactor. This model predicted the following quantities along the axial distance: monomer conversion, reaction mixture temperature and pressure, mass fraction of oxygen, peroxides, monomer, radicals and polymer; average molecular weights, long and short chain branching frequencies; Peclet, Nusselt, Reynolds and Prandtl numbers, global heat-transfer coefficient, velocity, viscosity and specific heat.

The model presented in this work is the continuation of an update process of the reduced model by Asteasuain, Pereda, et al. (2001). First the prediction of the complete MWD of the polymer was included in a gPROMS implementation of the model. Preliminary results can be found in Asteasuain and Brandolin (2006). Now, in a second stage, we finish the update by incorporating the prediction of the short and long branching indexes in the gPROMS model. This software presents several advantages, in particular its capability of solving complex optimization problems. The following basic hypothesis and features of the reduced model by Asteasuain, Pereda, et al. (2001) were kept: plug flow, reaction mixture forming a single supercritical phase, variation of physical and transport properties along the axial length and the use of the heat-transfer equations specially developed for this type of reactor (Lacunza et al., 1998). A typical reactor configuration, showing different jacket zones and lateral feedings, is displayed in Fig. 1.

Table 1
Kinetic mechanism

Peroxide initiation	$I_{m,x} \xrightarrow{k_{m,x}} 2R(0)$	(1)
Oxygen initiation	$O_2 + M \xrightarrow{k_o} 2R(0)$	(2)
Monomer thermal initiation	$3M \xrightarrow{k_{mi}} R(1) + R(2)$	(3)
Generation of inert	$O_2 + R(m) \xrightarrow{f_o k_o} X$	(4)
Propagation	$R(m) + M \xrightarrow{k_p} R(m+1)$	(5)
Termination by combination	$R(n) + R(m) \xrightarrow{k_{tc}} P(n+m)$	(6)
Thermal degradation	$R(m) \xrightarrow{k_{tdt}} P(m) + R(0)$	(7)
Chain transfer to monomer	$R(m) + M \xrightarrow{k_{trm}} P(m) + R(1)$	(8)
Chain transfer to polymer	$R(n) + P(m) \xrightarrow{mk_{trp}} P(n) + R(m)$	(9)
Chain transfer to transfer agent	$R(m) + S \xrightarrow{k_{trs}} P(m) + R(0)$	(10)
Backbiting	$R(m) \xrightarrow{k_{bb}} R(m)$	(11)
β-Scission of secondary radical	$R(m) \xrightarrow{k_{\beta 1}} P(m) + R(0)$	(12)
β-Scission of tertiary radical	$R(m) \xrightarrow{k_{\beta}} P(m) + R(0)$	(13)

Table 1 shows the kinetic mechanism considered in this model. Oxygen (O_2) and organic peroxide (I) initiation, and monomer (M) thermal initiation (Eqs. (1)–(3)) generate radicals when the reactor temperature reaches appropriate levels. Propagation reaction (Eq. (5)) takes place when monomer reacts with radicals to produce a growing macromolecule. These macroradicals may be deactivated by oxygen, generating an inert (Eq. (4)). This reaction is important to obtain an accurate prediction of temperature peaks. Natural termination is produced by combination of two radicals (Eq. (6)) or by thermal degradation (Eq. (7)). Transfer agents (S) are commonly fed to the reactor to control the molecular weight. They react with radicals producing a polymer and an initiation radical (Eq. (10)). In consequence, the presence of transfer agents result in shorter molecules. Transfer to monomer (Eq. (8)) and polymer (Eq. (9)) are also important for the prediction of the molecular weights. Intramolecular

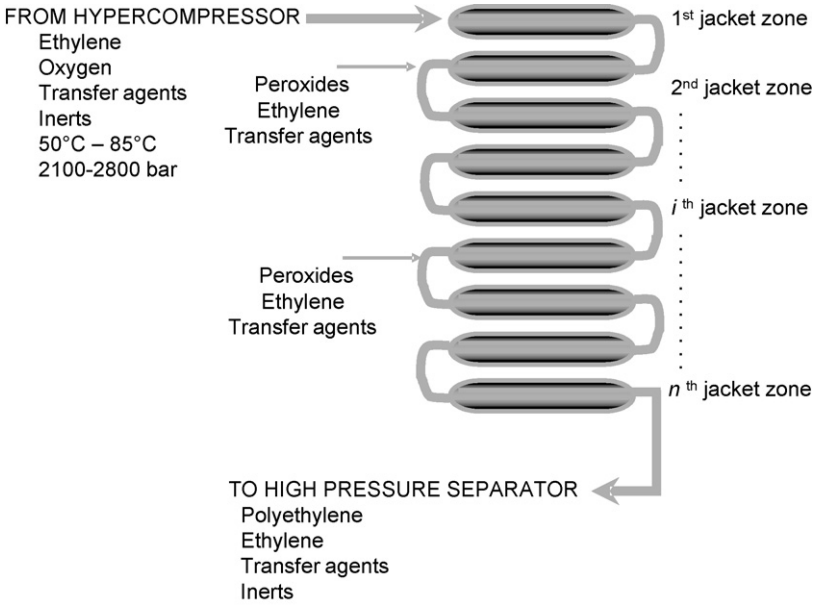

Fig. 1. Tubular reactor for high-pressure ethylene polymerization.

reactions (Eqs. (11)–(13)) affect the polymer branching. In Eq. (1), $I_{m,x}$ is the peroxide initiator mixture at the x-th lateral injection; in Eqs. (4)–(13), $P(m)$ and $R(m)$ are polymer and living radical molecules, respectively, of chain length m. The set of kinetic constants obtained in Asteasuain, Pereda, et al. (2001) are used here.

Eqs. (14)–(26) show the main model equations, which include mass and energy balances, balance equations for the moments and pgfs of the polymer and macroradical MWD, pressure drop along the reactor length, and algebraic equations for the monomer conversion and polymer molecular properties.

Global mass balance

$$\rho(z)v(z) = F_{\text{main}} + \int_0^z \sum_j \bar{F}_j(z)\,\mathrm{d}z \tag{14}$$

Mass balances of components

$$\frac{\mathrm{d}(C_j(z)v(z))}{\mathrm{d}z} = r_j(z) + \bar{F}_j(z)/\mathrm{Mw}_j \quad j = \mathrm{O_2}, M, I_{m,x}, S \tag{15}$$

Balances of branching, side groups, moments and pgfs

$$\frac{\mathrm{d}(\Psi(z)v(z))}{\mathrm{d}z} = r_\Psi(z) \quad \Psi = \mathrm{LCB, Me, Vi, Vd}, \lambda_a, \mu_a, \phi_{a,l}, \varphi_{a,l} \tag{16}$$

Energy balance

$$\rho(z)v(z)C_{\mathrm{p}}(z)\frac{\mathrm{d}T(z)}{\mathrm{d}z} = -\frac{4U(z)(T(z)-T_{\mathrm{j}})}{D} + r_{\mathrm{pm}}(z)(-\Delta H) + \check{C}\mathrm{p}(T_{\text{inlet}} - T(z))\sum_j \bar{F}_j(z) \tag{17}$$

Pressure drop

$$\frac{\mathrm{d}P(z)}{\mathrm{d}z} = -\rho(z)\left(v(z)\frac{\mathrm{d}v(z)}{\mathrm{d}z} + \frac{2f_{\mathrm{f}}\,v(z)^2}{D}\right) \tag{18}$$

Number average molecular weight

$$\mathrm{Mn}(z) = \mathrm{Mw}_M \frac{\lambda_1(z)+\mu_1(z)}{\lambda_0(z)+\mu_0(z)} \tag{19}$$

Weight average molecular weight

$$\mathrm{Mw}(z) = \mathrm{Mw}_M \frac{\lambda_2(z)+\mu_2(z)}{\lambda_1(z)+\mu_1(z)} \tag{20}$$

Short chain branches/1000 C

$$\frac{\mathrm{SCB}}{1000\mathrm{C}}(z) = \frac{500\,\mathrm{Me}(z)}{\mu_1(z)+\lambda_1(z)} \tag{21}$$

Long chain branches/1000 C

$$\frac{\mathrm{LCB}}{1000\mathrm{C}}(z) = \frac{500\,\mathrm{LCB}(z)}{\mu_1(z)+\lambda_1(z)} \tag{22}$$

Vinyl groups/1000 C

$$\frac{\mathrm{Vi}}{1000\mathrm{C}}(z) = \frac{500\,\mathrm{Vi}(z)}{\mu_1(z)+\lambda_1(z)} \tag{23}$$

Vinylidene groups/1000 C

$$\frac{\mathrm{Vd}}{1000\mathrm{C}}(z) = \frac{500\,\mathrm{Vd}(z)}{\mu_1(z)+\lambda_1(z)} \tag{24}$$

Monomer conversion

$$x(z) = 1 - \frac{v(z)C_M(z)\mathrm{Mw}_M}{F_{M,\text{main}} + \int_0^z \bar{F}_M(z)\,\mathrm{d}z} \tag{25}$$

Polymer MWDs

$$n(m,z) = f(\varphi_{0,l}(z)),\ w(m,z) = f(\varphi_{1,l}(z)),\ c(m,z) = f(\varphi_{2,l}(z)) \tag{26}$$

In these equations, ρ and C_{p} are the density and heat-capacity of the reaction mixture, v is the axial velocity, T and T_{j} are the reactor and jacket temperatures, and P is the reactor pressure; U, D, ΔH, f_{f} and Mw_j are the global heat-transfer coefficient, reactor internal diameter, propagation reaction enthalpy, friction factor and molecular weight of the j component; λ_a and μ_a are the a th order moments of the radical and polymer chain length distribution; LCB, Me, Vi and Vd are the concentration of long chain branches and methyl, vinyl and vinylidene groups; r_j and r_Ψ are the generation rate of the j and Ψ entities, respectively; r_{pm} is the reaction rate of the propagation reaction; F_{main} and $F_{M,\text{main}}$ are the global and monomer mass fluxes at the reactor entrance, respectively; $\bar{F}_j$ is the mass flow per unit area and unit length of the j component; $\phi_{a,l}$ and $\varphi_{a,l}$ are the probability generating functions (pgf) of the radical and polymer chain length distribution ($a = 0, 1, 2$ is related to the MWD expressed in number, weight and chromatographic (mass times the molecular weight) fraction, respectively, as will be explained later, and l is the dummy variable of the pgf); $n(m,z)$, $w(m,z)$ and $c(m,z)$ are the number, weight and chromatographic fraction of the macromolecule of chain length m. Expressions corresponding to the terms r_j for the reaction components and r_Ψ for Ψ = Me, Vi and Vd can be found in Brandolin et al. (1996). The expression for r_{LCB} and also for the long chain branches/1000 C (Eq. (22)) follow the approach proposed by Pladis and Kiparissides (1998). Balance equations for the distributions' moments and pgfs can be found in Appendix A. pgfs balance equations will be described later. The molar flows per unit area and unit length $\bar{F}_j$ are used to model the lateral feedings to the reactor as explained below.

2.1. Modeling of lateral feedings

Mass and energy balances for a steady-state, plug flow tubular reactor without axial dispersion lead to a set of ordinary differential equations in which the independent variable is the axial length (z). Process conditions at the reactor entrance (z_0) determine the set of initial conditions for the differential equations. In this context, a lateral injection at a given point z_i mathematically represents an instantaneous addition (an impulse function) of mass and energy to the system, which cause discontinuities in the values at that point of the differential variables involved (i.e. sudden changes in mass flow, concen-

trations and/or temperature). A usual approach to model this situation is to integrate the differential equations up to the point z_i; mass and energy balances are then applied for the mixing of the lateral injection with the reactor outlet at that point, and the result is used as new initial conditions to continue with the integration of the differential equations. However, the implementation of this procedure is not straightforward in gPROMS because this software assumes a priory that all differential variables are continuous (Process Systems Enterprise, Ltd., 2005). Although discontinuities in differential variables can be forced in simulation mode, this cannot be extended to optimization problems. Therefore, another approach is used in this work to model the lateral feedings. It consists in adding an extra term to the mass and energy balances ($\bar{F}_j(z)/\mathrm{Mw}_j$ in Eq. (15) and $\check{C}\mathrm{p}(T_{\mathrm{inlet}} - T(z))\sum_j \bar{F}_j(z)$ in Eq. (17)), representing the side addition to the system. A molar flow per unit length ($\bar{F}_j(z)$) that is non-zero only in a very short length interval starting at the injection point, is used to approximate the impulse function of the lateral injection. The side addition term $\bar{F}_j(z)$ is calculated according to:

$$A\frac{\bar{F}_j(z)}{\mathrm{Mw}_j}\Delta z = \text{side molar flow rate of component } j \tag{27}$$

where A is the reactor cross-sectional area and Δz is the length interval in which $\bar{F}_j(z)$ is non-zero. The side addition term is not included in the balances of moments and pgfs of the radical and polymer MWDs (Eq. (16)) because its value is always zero in these cases, as the lateral feedings never contain polymer or macroradicals. The global mass balance is formulated as an algebraic equation (Eq. (14)), because it was found that numerical problems in the integration of the algebraic-differential system appeared, at the points corresponding to the lateral additions, when this balance was formulated as a differential equation.

With this approach, the lateral feedings are included in the model equations and therefore no special procedure in the integration of the differential equations is needed. The differential variables involved keep their continuity property, but choosing Δz small enough the step changes in their values can be reasonably approximated. Numerical experiments were carried out in order to find an appropriate length interval Δz. Results of the gPROMS model were corroborated with the ones of our previous model, implemented in FORTRAN using the discontinuous integration approach.

2.2. Modeling of the complete MWD

In order to model the MWD in this process we use the probability generating function (pgf) technique (Asteasuain, 2003; Asteasuain, Brandolin, et al., 2002; Asteasuain, Sarmoria, et al., 2002). The pgf transformation is applied to the infinite set of mass balance equations of the macromolecular species $P(m)$ and $R(m)$ ($m = 1, \ldots, \infty$), leading to a finite set of equations where the dependent variable is the pgf transform of the MWD ($\phi_{a,l}$ and $\varphi_{a,l}$). The pgf calculated by solving the transformed equations, are then inverted to recover the MWD. pgfs are defined for each macromolecule as shown in Eqs. (28) and (29)

$$\phi_{a,l} = \sum_{m=1}^{\infty} l^m \frac{m^a R(m)}{\lambda_a} \tag{28}$$

$$\varphi_{a,l} = \sum_{m=1}^{\infty} l^m \frac{m^a P(m)}{\mu_a} \tag{29}$$

where $a = 0, 1, 2$

We have defined three types of pgf, identified by subscript $a = 0, 1, 2$ in the above equations, which represent the pgf transforms of the MWD expressed as number fraction versus molecular weight ($n(m)$), weight fraction versus molecular weight ($w(m)$) or the product of weight fraction and molecular weight versus molecular weight ($c(m)$). Inversion of each type of pgf allows the recovery of the three kinds of distribution independently, attenuating in this way numerical noise propagation (Brandolin et al., 2001).

The mass balances corresponding to macromolecules $P(m)$ and $R(m)$ (see Appendix A) can be transformed into the pgf domain in a simple way by means of the pgf Transform Table we have previously developed (Asteasuain, 2003; Asteasuain, Sarmoria, et al., 2002). The resulting terms (r_Ψ in Eq. (16), $\Psi = \phi_{a,l}, \varphi_{a,l}$) are shown in Appendix A. The pgf inversion algorithm employed in this model is an adaptation of the Stehfest algorithm for Laplace transform inversion (Asteasuain, 2003). The equations corresponding to this inversion algorithm are

$$d_a(m) = \frac{\ln 2}{m}\sum_{j=1}^{J} K_j\, \varphi_{a,\, l=\mathrm{e}^{-j(\ln 2/m)}} \qquad a = 0, 1, 2 \tag{30}$$

where $d_0(m)$, $d_1(m)$ and $d_2(m)$ are the MWDs $n(m)$, $w(m)$ and $c(m)$, respectively, and

$$K_j = (-1)^{j+J/2} \sum_{k=[(j+1)/2]}^{\min(j,J/2)} \frac{k^{J/2}(2k)!}{(J/2-k)!k!(k-1)!(j-k)!(2k-j)!} \tag{31}$$

where J is an even integer. This is a parameter of the inversion method. A methodology for selecting an appropriate value for this parameter, and other details about this and other alternative inversion methods can be found elsewhere (Asteasuain, 2003; Asteasuain, Brandolin, et al., 2002).

Eqs. (30) and (31) are the algebraic equations involved in Eq. (26). The pgf balance equations (Eq. (16), $\Psi = \phi_{a,l}, \varphi_{a,l}$) are formulated for the values of the dummy variable l required by Eq. (30), which are function of the chain length values where it is desired to predict the MWD (m in Eq. (30)). It should be noted that pgfs are calculated and inverted at each point along the axial distance (z), and therefore the MWDs $n(m)$, $w(m)$ and $c(m)$ are obtained as function of z. Eq. (31) involves large quotients of factorials leading to coefficients of alternating sign. In order to minimize possible numerical noise, these coefficients were computed with a procedure developed in FORTRAN code, which uses special built-in functions to calculate the factorials. The FORTRAN procedure was linked to gPROMS using the Foreign Object interface of this software.

3. Reactor optimization

3.1. Case I

One of the most important problems encountered in operating a polyethylene reactor of fixed size is to select the optimum operating conditions that maximize the reactor productivity at the desired product quality (Mavridis & Kiparissides, 1985). As many polymer properties are closely related to the MWD, it is of significant economic importance to maximize conversion as well as achieving a desired MWD. Besides, long and short branching frequencies are also key molecular parameters in defining the polymer quality. This case study aims at maximizing monomer conversion while maintaining the grade specifications of the Base Case polymer. These specifications are defined in terms the complete MWD and branching frequencies. The Base Case operating point is summarized in Table 2. All design and operating variables listed in this table (location of lateral feedings, flow rates, inlet pressure and inlet and jacket temperatures) are considered as optimization variables. The lower and upper bounds for each of these 21 optimization variables were selected from the usual operating range of a typical industrial reactor.

In a first approach to this case study (Case I*a*), only constraints on the deviation from the complete MWD of the Base Case polymer were included in the optimization problem as polymer quality requirements. The mathematical formulation of the optimization problem of this case is shown in Eqs. (32a)–(32g) and (32j). In this set of equations, Eqs. (32c) and (32d) represent the maximum allowed deviation with respect to the Base Case weight and chromatographic MWDs. The path constraint represented by Eq. (32e), an upper bound on the reaction mixture temperature along the axial distance, was imposed to ensure safe operating conditions, as thermal runaway occurs at 345 °C (Kiparissides, Verros, & Pertsinidis, 1994). Eq. (32f) represents an upper bound for the reactor temperature at the reactor exit, required for downstream process units. Eq. (32g), in which variable A is the cross-sectional area of the reactor, involves a constraint in the total monomer feed to the reactor (main feed plus lateral feedings), so as to keep the same total monomer feed rate as in the Base Case. Values of the lower and upper bounds u^L and u^U are presented in Section 4.2.1, where the results for Case I are discussed.

Table 2
Base Case operating conditions

Inlet temperature (°C)	77
Inlet pressure (bar)	2300
Oxygen. Main feed (kg/s)	6.9×10^{-5}
Transfer agent. Main feed (kg/s)	0.00762
Transfer agent. 1st lateral injection (kg/s)	0
Transfer agent. 2nd lateral injection (kg/s)	0
Peroxide. 1st lateral injection (kg/s)	0.00102
Peroxide. 2nd lateral injection (kg/s)	1.57×10^{-4}
Monomer. Main feed (kg/s)	11
Monomer. 1st lateral injection (kg/s)	0
Monomer. 1st lateral injection (kg/s)	0
Location of 1st lateral injection (z/L)	0.12
Location of 2nd lateral injection (z/L)	0.63
Jacket temp. Zones 1–8 (°C)	170-225-170-170-170-170-170-170
Conversion (%)	25
SCB/1000 C	24.7
LCB/1000 C	2.14

As shown in Section (4) even with tight constraints on the deviation from the original MWD such as those imposed in Case I*a*, short and long chain branching may deviate considerably from their original values. Hence, since the level of branching may be relevant to the polymer properties, another optimization problem was solved. This new case is referred to as Case I*b*. Here, constraints on short and long chain branching frequencies were added to the previous optimization problem (Eqs. (32h) and (32i)). These constraints allowed deviations of up to 5% from the corresponding Base Case values.

Both Case I optimizations were solved using the commercial software gPROMS (Process Systems Enterprise, Ltd.). Finally, a comparative analysis of the results was performed.

$$\max_u x(z_{\max}) \tag{32a}$$

$$\text{s.t.} \quad \text{Model algebraic} - \text{differential system} \tag{32b}$$

$$\sum_i \left(\frac{w_{\text{new}}(m_i, z_{\max}) - w_{\text{Base Case}}(m_i)}{w_{\text{Base Case}}(m_i)} \right)^2 \leq 0.01 \tag{32c}$$

$$\sum_i \left(\frac{c_{\text{new}}(m_i, z_{\max}) - c_{\text{Base Case}}(m_i)}{c_{\text{Base Case}}(m_i)} \right)^2 \leq 0.01 \tag{32d}$$

$$T(z) \leq 335\,^\circ\text{C} \tag{32e}$$

$$T(z_{\max}) \leq 285\,^\circ\text{C} \tag{32f}$$

$$A \left(F_{M,\text{main feed}} + \int_0^z \bar{F}_M(z)\,\text{d}z \right) = 11\,\text{kg/s} \tag{32g}$$

$$23.5 \leq \text{SCB}/1000\text{C}(z_{\max}) \leq 26 \tag{32h}$$

$$2 \leq \text{LCB}/1000\text{C}(z_{\max}) \leq 2.25 \tag{32i}$$

$$u^L \leq u \leq u^U \tag{32j}$$

3.2. Case II

Another important goal in polymer engineering is tailoring the polymer MWD by proper manipulation of the operating conditions. This case study involved the optimization of the operating conditions in order to synthesize a polymer with a new, specific MWD. In order to challenge the present optimization framework, the target was to achieve a bimodal MWD with a constrained polydispersity. Bimodal MWDs are rarely observed in typical operation of tubular reactors (Kim & Iedema, 2004), and there are few works reporting operating conditions leading to this type of distributions (Asteasuain & Brandolin, 2006; Kim & Iedema, 2004). The same set of optimization variables as in the previous case was maintained. The optimization formulation is presented in Eq. (33).

$$\max_u c_{\text{calc}}(m_3, z_{\max}) - c_{\text{calc}}(m_2, z_{\max}) \tag{33a}$$

s.t.

$$\text{Model algebraic} - \text{differential system} \tag{33b}$$

$$c_{\text{calc}}(m_2, z_{\max}) - c_{\text{calc}}(m_1, z_{\max}) \leq 0 \tag{33c}$$

$$c_{\text{calc}}(m_2, z_{\max}) - c_{\text{calc}}(m_3, z_{\max}) \leq 0 \tag{33d}$$

$$\text{Pd}(z_{\max}) \leq 9 \tag{33e}$$

$$x(z_{\max}) \geq 0.2 \tag{33f}$$

$$T(z) \leq 335\,^{\circ}\text{C} \tag{33g}$$

$$T(z_{\max}) \leq 285\,^{\circ}\text{C} \tag{33h}$$

$$A\left(F_{M,\text{main feed}} + \int_0^z \bar{F}_M(z)\,\text{d}z\right) = 11\,\text{kg/s} \tag{33i}$$

$$u^L \leq u \leq u^U \tag{33j}$$

A necessary condition for a MWD to be bimodal, that is, with two peaks, is the existence of a local minimum in the distribution curve between the peaks. Hence, one way of enforcing bimodality is to ensure the existence of a minimum in the MWD. In this case study, a bimodal MWD was designed so as to have a local minimum within the chain length interval $[m_1, m_3]$. This was specified by the constraints represented by Eqs. (33c) and (33d). These constraints imply that the value of the MWD at the chain length m_2, $m_2 \in [m_1, m_3]$, must be lower than its value at the chain lengths m_1 and m_3, and therefore that there has to be a minimum between m_1 and m_3. The optimization aimed at maximizing the height of the right peak of the distribution, measured as indicated by Eq. (33a). Chain length values m_1, m_2 and m_3 were selected so that the corresponding molecular weights ($m_i \text{Mw}_M$) were, respectively, 44,380, 224,000 and 280,000 g/mol. It should be noted that several other requirements on the MWD might have been specified, such as a different modality, location and/or height of the curve peaks, or even a complete MWD. A constraint on the polydispersity was included to limit the broadness of the distribution (Eq. (33e)). Eq. (33f) was included in order to exclude operating conditions leading to too low conversion values. Lower and upper bounds for the optimization variables (u^L and u^U) are shown in Section 4.2.2, where the results corresponding to this case are discussed.

4. Results and discussion

4.1. Model validation

Our former FORTRAN model of the reactor had already been thoroughly validated against industrial data (Asteasuain, Pereda, et al., 2001). Therefore, the gPROMS model was compared with the former one for those variables predicted by both of them. First of all, numerical experiments were carried out in order to find a suitable value for the length interval Δz employed to model the lateral feedings. A value of $\Delta z = 0.001$ m was found to be appropriate. Excellent agreement between both models was achieved. As an example, Fig. 2 shows the initiator mass fraction profiles for the former and the gPROMS models, corresponding to the Base Case operating conditions listed in Table 2. Notice that peroxide initiators are, in this case, the only reactants injected through the lateral feedings. The first peroxide mixture (peroxide mixtures are modeled as single fictitious species) is injected at $z/L = 0.12$, and the second peroxide mixture is injected at $z/L = 0.63$. As can be seen, the methodology employed to model the lateral feedings allowed obtaining the same results as with the former model. Comparison of some major output variables, such as the number and weight average molecular weights, conversion, reactor temperature and branching, are presented in Table 3 and in Fig. 3. gPROMS simulation results did not vary for smaller values of Δz or for smaller tolerance settings for the ODE solver. The slight differences with respect to the results of the FORTRAN model should be attributed to specific implementation issues, such us the different numerical solvers available for each software.

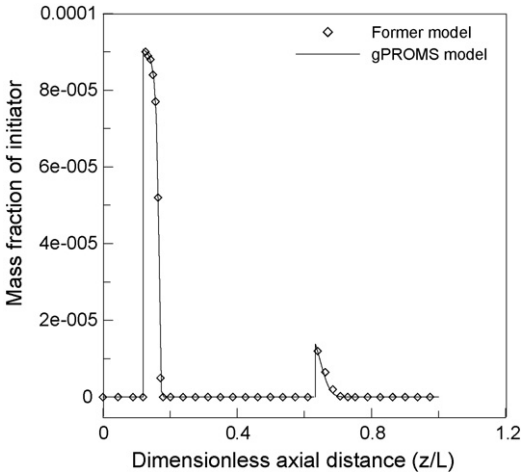

Fig. 2. Comparison between the peroxide initiator mass fraction profiles calculated with the former model and with the gPROMS model of the polymerization reactor.

Since experimental MWDs are not available to compare with the theoretical predictions, we operate with them in order to calculate parameters that are available, such us Mn and Mw. The reactor model calculates, independently from the predicted

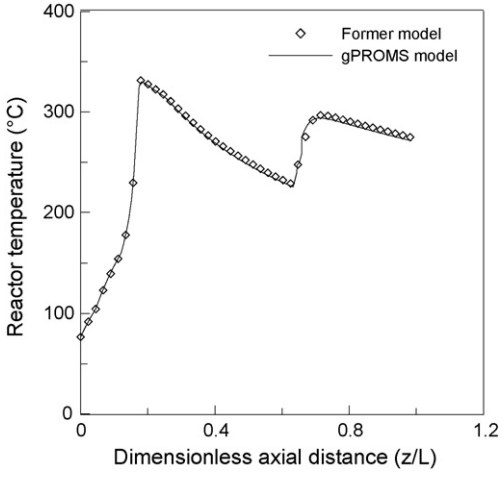

Fig. 3. Comparison between the temperature profile calculated with the former polymerization reactor model and with the corresponding gPROMS model.

Table 3
Comparison between the final values of the number average molecular weight (Mn), weight average molecular weight (Mw), conversion, long chain branches per 1000 carbon atoms (LCB/1000 C) and short chain branches per 1000 carbon atoms (SCB/1000 C) calculated with the former FORTRAN model and with the gPROMS model

	Mn	Mw	Conversion	LCB/1000 C	SCB/1000 C
Former model	21,427	160,542	25.3	2.13	23.7
gPROMS model	21,839	161,491	25.7	2.14	24.7

Table 4
Comparison between average molecular weights calculated from the recovered MWD (Mn^d; Mw^d) and by the method of the moments (Mn^m; Mw^m)

Case	Mn^d (g/mol)	Mn^m (g/mol)	Relerr %	Mw^d (g/mol)	Mw^m (g/mol)	Relerr %
Base Case	20,500	21,600	−12.21	170,900	162,900	−0.57
Case05	22,100	23,600	−8.00	197,900	199,800	3.43
Case06	23,700	25,500	3.85	204,100	207,400	6.85
Case10	18,200	18,700	−6.92	131,100	126,800	13.06

The *Relerr* column gives the percent relative error of the average molecular weights calculated from the MWD with respect to the experimental data [100(calc-exp)/exp].

MWDs, these average molecular weights by the well-known method of the moments (Eqs. (20) and (25)). Table 4 presents a comparison between the values of Mn and Mw calculated by the method of the moments and those obtained from the predicted MWDs, in both cases rounded to the nearest hundred. The relative error of the average molecular weights calculated from the MWD with respect to the experimental data is also presented. The experimental data correspond to the operating conditions of the Base Case (see Table 2), and of the cases named Case05, Case06 and Case10. Operating conditions for the three last cases can be found in Asteasuain, Pereda, et al. (2001). As can be seen, the average molecular weights calculated from the MWDs are very similar to the ones calculated by the method of the moments. Besides, the relative error with respect to the experimental values is usually less than 10%. It is true that, for a single case, comparing the average molecular weights obtained from a calculated MWD with their experimental counterparts would not be a suitable method of validating the model output, because it is possible that two different MWDs may have the same average molecular weights, and therefore a wrongly predicted MWD may lead to the correct values of Mn and Mw. However, it is very unlikely that this happens in several instances of the same process. As similar agreement was observed at many other operating conditions apart from the ones presented in Table 4, we believe that this excludes the possibility of wrong MWD giving correct average molecular weights.

4.2. Reactor optimization

4.2.1. Case I

Table 5 shows the optimization results for Case I*a*. It also contains the lower and upper bounds of the optimization variables used for Eq. (32j). An increase in monomer conversion from 25% (See Table 2) to 32% is achieved, which is economically very significant due to the high throughput of the reactor. At the same time, the original MWD is maintained, as can be observed in Fig. 4. Significant differences can be noted with respect to the Base Case operating point. For instance, the first lateral feeding is nearer to the reactor entrance, and the monomer feed is split up to the maximum allowed limit towards the lateral feedings. Besides, there is no transfer agent in the main feed, but this reactant is only fed through the lateral feedings. This is an interesting result, because transfer agents are only included in the main feed under usual operation of these reactors (Kim & Iedema, 2004). The advantage of the lateral feeding policy of the transfer agent over the usual operation is supported by previous optimization studies on this reactor (Asteasuain & Brandolin, 2006). In that work, maximum conversion was sought for the same process constraints, but with transfer agent addition restricted to the main feed. The maximum conversion obtained in that work was lower than the one obtained here with lateral feeding of the transfer agent. It can be noted that the overall transfer agent flow rate is considerably higher at the optimal point. This is consistent

Table 5
Optimal operating conditions and bounds for Case Ia

Variable	Optimum	L. bound	U. bound
Inlet temperature (°C)	66	65	85
Inlet pressure (bar)	2600	2100	2800
Oxygen. Main feed (kg/s)	8.9×10^{-5}	10^{-5}	8.9×10^{-5}
Transfer agent. Main feed (kg/s)	0	0	0.9
Transfer agent. Lat. injs. (1st–2nd) (kg/s)	0.16–0.22	0–0	0.9–0.9
Peroxide. 1st lat. inj. (kg/s)	6.6×10^{-4}	6.9×10^{-5}	0.0017
Peroxide. 2nd lat. inj. (kg/s)	1.6×10^{-4}	6.9×10^{-5}	0.0017
Monomer. Main feed (kg/s)	6.5	6.5	11
Monomer. Lat. injs. (1st–2nd) (kg/s)	2.7–1.8	0–0	4.5–4.5
Location of lat. injs. (1st–2nd) (z/L)	0.04–0.63	0.03–0.38	0.12–0.63
Jacket temp. Zones 1–8 (°C)	270–164	150	270
	150–150		
	150–150		
	150–159		
Conversion (%)	32		
SCB/1000 C	18.9		
LCB/1000 C	2.73		

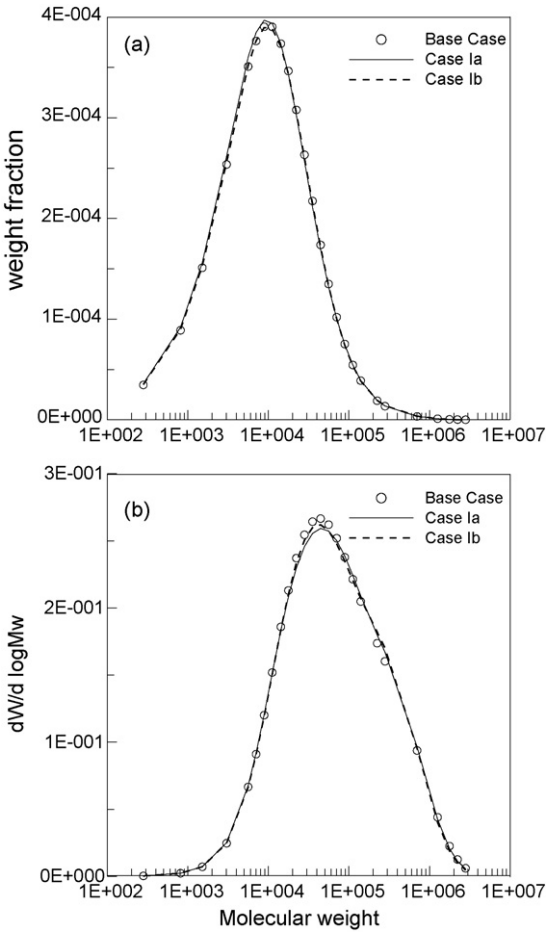

Fig. 4. Comparison of MWDs corresponding to the Base Case and to the optimal operating conditions of Case Studies I*a* and I*b*.

with previous studies on this reactor (Asteasuain & Brandolin, 2006; Asteasuain, Ugrin, et al., 2001), which showed that higher amounts of transfer agent are needed in order to achieve higher conversions while maintaining the same molecular weights.

The reactor temperature profile corresponding to the optimal point of Case I*a* is plotted in Fig. 5. It can be seen that the path

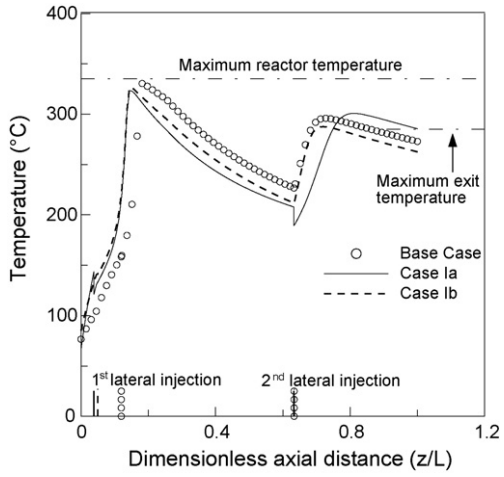

Fig. 5. Reactor temperature profiles corresponding to the Base Case and to the optimal operating conditions of Case Studies I*a* and I*b*.

and end point constraints on the reactor temperature (Eqs. (32e) and (32f)) are satisfied, although the outlet temperature is at its upper bound. The decrease in the reactor temperature observed at the lateral injection points is due to the lower temperature of the lateral feedings, whose value is the same as the main feed one. The slope of the reactor temperature profile corresponding to the optimal point is steeper near the reactor entrance than for the Base Case, in order to reach the appropriate temperature for peroxide addition in the shorter length previous to the lateral feed. This steep profile is achieved with a high jacket temperature in the first jacket zone, as seen in Table 5.

Although MWD requirements were satisfied in Case I*a*, differences on short and long chain branching with respect to the correspondent Base Case values were of −24% and +28%, respectively (see Tables 2 and 5). As branching frequencies are, together with the overall MWD, important in defining the polymer properties, these changes might imply a different behavior of the new resin. Therefore, Case I*b* was solved, adding constraints on the short and long branching deviations. Upper and lower bounds employed in Eq. (32j) are shown in Table 6. Results corresponding to the optimization variables, conversion and branching at the optimal points are also shown in this table. It can be seen that now branching frequencies lie between the desired bandwidth of ±5% of their Base Case values. The original MWD is also maintained, as shown in Fig. 4. The new requirements on branching frequencies are achieved at the expense of a 4% reduction in the optimal conversion, but there is still a 3% increase with respect to the Base Case value. The locations of the lateral feedings are similar to the ones in Case I*a*, but both peroxide flow rates are higher. The inlet pressure is lower, and so less transfer agent is needed to keep the molecular weights of the Base Case polymer. It can also be observed that now no monomer is deviated to the lateral feedings.

Table 6
Optimal operating conditions and bounds for Case Ib

Variable	Optimum	L. bound	U. bound
Inlet temperature (°C)	85	65	85
Inlet pressure (bar)	2100	2100	2800
Oxygen. Main feed (kg/s)	8.9×10^{-5}	10^{-5}	8.9×10^{-5}
Transfer agent. Main feed (kg/s)	0	0	0.9
Transfer agent. Lat. injs. (1st–2nd) (kg/s)	0.099–0.05	0–0	0.9–0.9
Peroxide. 1st lat. inj. (kg/s)	1.3×10^{-3}	6.9×10^{-5}	0.0017
Peroxide. 2nd lat. inj. (kg/s)	2.8×10^{-4}	6.9×10^{-5}	0.0017
Monomer. Main feed (kg/s)	11	6.5	11
Monomer. Lat. injs. (1st–2nd) (kg/s)	0–0	0–0	4.5–4.5
Location of lat. injs. (1st–2nd) (z/L)	0.05–0.63	0.03–0.38	0.12–0.63
Jacket temp. Zones 1–8 (°C)	270–171	150	270
	150–150		
	150–150		
	150–150		
Conversion (%)	29		
SCB/1000 C	23.5	23.5	26
LCB/1000 C	2.25	2	2.25

The temperature profile is shown in Fig. 5. As previously, path and end point constraints are satisfied. This profile is similar to the one of the previous case up to the peak and slightly higher in the cooling zone. The rise after the second peroxide addition is steeper, due to the higher peroxide flow rates. However, as a consequence of the higher temperature, peroxides are consumed sooner and hence the second reaction zone (up to the second temperature peak) is shorter.

4.2.2. Case II

The Case II involved tailoring the polymer MWD in order to obtain a bimodal distribution. Fig. 6 shows the MWD for the optimal operating point corresponding to this case. It can be seen that bimodal distribution is achieved at the reactor exit, with a minimum within the chain length interval $[m_1, m_3]$, as required in the optimization problem (see Section 3.2). Fig. 6 also shows the MWD before the second lateral addition. This shows that the polymer produced in the first reaction zone provides with the high molecular weight portion of the bimodal distribution. Hence, low molecular weight material is formed in the second reaction zone, leading to the final bimodal distribution.

The optimal operating scenario is presented in Table 7, as well as the upper and lower bounds of the optimization variables employed in Eq. (33j). Notice that an important addition of transfer agent at the second injection is employed. Clearly, this aids in achieving the low molecular weight polymer produced after this point. On the contrary, operating conditions in the first reaction zone are appropriate for synthesizing the high molecular weight polyethylene. Transfer agent flow rate in the main feed is slightly smaller than for the Base Case, and the reactor temperature is markedly lower, as shown in Fig. 7. The jacket temperature is low at the beginning of the first reaction zone, in order to reduce the reactor temperature. Then it is raised towards the end of this zone, and also towards the end of the second one, to maintain a sufficiently high reaction rate so as to reach the desired conversion. Reaction zones are longer than in the Base Case, to allow obtaining an appropriate conversion level under the lower reaction temperatures. Another interesting feature is the small split of the monomer feed to the second lateral injection. If there is no such split, the MWD of the polymer produced after the first reaction zone will have a similar shape to the one shown in Fig. 6 (dashed line), but the distribution will be broader and the peak will reach the same height as the left shoulder (Fig. 8). This turns into a less pronounced bimodality in the final distribution (It must be kept in mind that the objective of the optimization problem is to maximize the height of the right peak). Besides, if the split is not present, the polydispersity at the reactor exit will reach a value of 10, which does not satisfy the constraint on this variable (Eq. (33e)). Without this constraint, the optimal solution can be quite different. Asteasuain and Brandolin (2006) found operating conditions leading to a bimodal distribution without polydispersity restrictions. Results of that work showed that, as in the present case, high molecular weight polymer was produced in the first reaction zone and low molecular weight polymer in the second one. However, the difference between the molecular weights of each zone was more

Table 7
Optimal operating conditions and bounds for Case II

Variable	Optimum	L. bound	U. bound
Inlet temperature (°C)	85	65	85
Inlet pressure (bar)	2173	2100	2800
Oxygen. Main feed (kg/s)	8.9×10^{-5}	10^{-5}	8.9×10^{-5}
Transfer agent. Main feed (kg/s)	0.064	0	0.9
Transfer agent. Lat. injs. (1st–2nd) (kg/s)	0–0.61	0–0	0.9–0.9
Peroxide. 1st lat. inj. (kg/s)	8.5×10^{-5}	6.9×10^{-5}	0.0017
Peroxide. 2nd lat. inj. (kg/s)	6.9×10^{-5}	6.9×10^{-5}	0.0017
Monomer. Main feed (kg/s)	10.2	6	11
Monomer. Lat. injs. (1st–2nd)(kg/s)	0–0.8	0–0	4.5–4.5
Location of lat. injs. (1st–2nd) (z/L)	0.03–0.62	0.03–0.38	0.12–0.63
Jacket temp. Zones 1–8 (°C)	270–150	150	270
	270–266		
	150–150		
	159–270		
Conversion (%)	20	20	
Pd	9		9

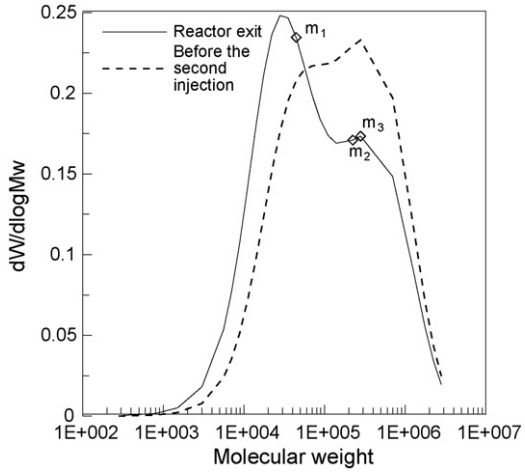

Fig. 6. MWD for the second case study.

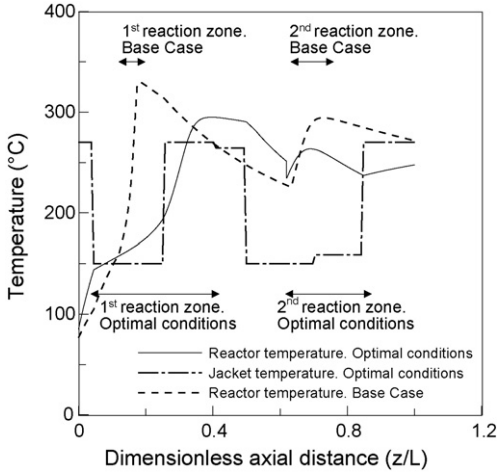

Fig. 7. Temperature profiles. Second case study.

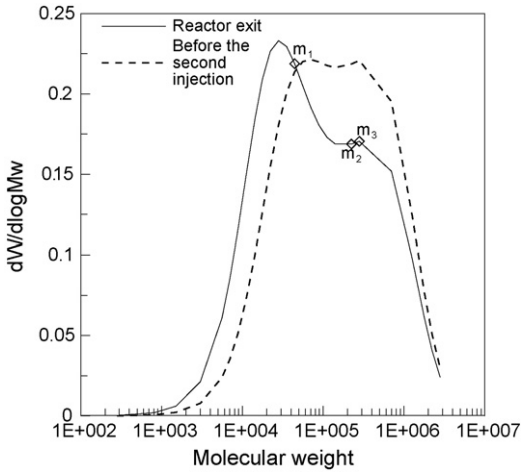

Fig. 8. MWD for the second case operating conditions without monomer split.

pronounced, leading to a polydispersity of around 18. Differences in the operating conditions obtained in Asteasuain and Brandolin (2006) with respect to the ones obtained here are, for instance, a greater amount of monomer deviated to the second lateral feeding, reducing the polymerization rate and heat generation in the first reaction zone, which results in lower temperatures. Also, the transfer agent flow rate was higher in the second lateral injection, which was moved towards the highest temperature zone of the reactor ($z/L = 0.38$), to achieve a high temperature second reaction zone.

The computational time required to solve the different optimization cases ranged between 2 and 5 h, in a personal computer with a Pentium IV processor of 3.0 GHz, and 1 Gb RAM.

5. Conclusions

A gPROMS implementation of a comprehensive steady-state model of the high-pressure ethylene polymerization in a tubular reactor was presented. This model, based on previous models by the authors, incorporated the prediction of the complete MWD as well as branching indexes as function of the reactor axial distance. Lateral feedings to the reactor, which mathematically involve discontinuities in differential variables, were successfully modeled by means of additional terms to the fundamental mass and energy balances. In this way, the model could be implemented within gPROMS optimization architecture. The model was validated with experimental data of average molecular weights and also against our former model, which had been successfully tested against information of an actual industrial reactor. Case studies involving tailoring of the MWD were presented. The first ones consisted in maximizing conversion while maintaining the MWD and branching of the polymer produced in a Base Case. When only the MWD was forced to be the same as the one of the Base Case, an increase in monomer conversion from 25% to 32% was achieved, with a negligible change in the polymer MWD. However, differences in short and long branches with respect to the Base Case were significant. The optimal operating point involved derivation of monomer to lateral feedings, and moving the first initiator injection towards the reactor entrance. Besides, transfer agent was only fed through the lateral injections. When deviations on short and long branches were also constrained, the maximum conversion was lower, but its increase was still important due to the high throughput of the reactor. In this case, monomer was not deviated to the lateral feedings, but transfer agent was still fed only through these points. In order to maintain the original molecular weight of the polymer, a higher transfer agent flow rate was needed as conversion increased, which is consistent with previous studies on this reactor.

The second case study involved finding operating conditions for synthesizing a polymer with a bimodal MWD of constrained polydispersity. The optimal operating point was very different to the usual ones for this kind of reactor, but this was not unexpected since bimodal MWD are seldom obtained. It was shown that operating conditions were designed so as to produce high and low molecular weight polymer in the first and second reaction zones, respectively, to finally compose the bimodal distribution. A low operating temperature and a considerable length distinguished the first reaction zone, while a high lateral feed rate of transfer agent characterized the second zone. Besides, a small split of the monomer feed to the second lateral addition was also required.

In view of the complex relationship existing between design and operating conditions, optimization studies are very useful tools for improving the performance of the reactor in terms of productivity and capability of tailoring the polymer molecular structure. Moreover, it was demonstrated that it is possible to produce new polymer grades with the high pressure tubular reactor. Polyethylene manufacturers may consider using the optimization approach presented in this paper not only to increase the process productivity but also to design novel polymer grades to satisfy specific market requirements.

Acknowledgements

The authors wish to thank Universidad Nacional del Sur (Bahía Blanca, Argentina), CONICET (Argentina) and Agencia Nacional de Promoción Científica y Tecnológica (Argentina) for financial support.

Appendix A

The mass balance for a polymer molecule of chain length m ($P(m)$) is (Brandolin et al., 1996)

$$\begin{aligned}\frac{\mathrm{d}(C_{P(m)}(z)v(z))}{\mathrm{d}z} &= \frac{1}{2}k_{\mathrm{tc}}(z)\sum_{r=1}^{m-1}C_{R(r)}(z)C_{R(m-r)}(z)(1-\delta_{m,0}-\delta_{m,1}) \\ &+ (k_{\mathrm{tdt}}(z)+k_{\beta 1}(z)+k_{\beta}(z))C_{R(m)}(z)(1-\delta_{m,0}) \\ &+ k_{\mathrm{trs}}(z)C_S(z)C_{R(m)}(z)(1-\delta_{m,0}) + k_{\mathrm{trp}}(z)\mu_1(z)C_{R(m)}(z) \\ &- k_{\mathrm{trp}}(z)\lambda_0(z)m\,C_{P(m)}(z)(1-\delta_{m,0}-\delta_{m,1}) \\ &+ k_{\mathrm{trm}}(z)C_M(z)C_{R(m)}(z)(1-\delta_{m,0}) \quad m=0,\ldots,\infty \end{aligned} \tag{A.1}$$

The mass balance for a macroradical of chain length m ($R(m)$) is (Brandolin et al., 1996)

$$\begin{aligned}\frac{\mathrm{d}(C_{R(m)}(z)v(z))}{\mathrm{d}z} &= k_{\mathrm{o}}(z)C_{O_2}(z)^{1.1}\,C_M(z)\delta_{m,0} + 2f_{I_1}k_{I_1}(z)C_{I_1}(z)\delta_{m,0} \\ &+2\,f_{I_2}k_{I_2}(z)C_{I_2}(z)\delta_{m,0}+k_{\mathrm{p}}(z)C_M(z)C_{R(m-1)}(z)(1-\delta_{m,0}) \\ &- k_{\mathrm{p}}(z)C_M(z)C_{R(m)}(z) + (k_{\mathrm{tdt}}(z)+k_{\beta 1}(z) \\ &+ k_{\beta}(z))\lambda_0(z)\delta_{m,0} + k_{\mathrm{trs}}(z)C_S(z)\lambda_0(z)\delta_{m,0} \\ &+ k_{\mathrm{trm}}(z)C_M(z)\lambda_0(z)\delta_{m,1} - k_{\mathrm{tc}}(z)\lambda_0(z)C_{R(m)}(z) \\ &- (k_{\mathrm{tdt}}(z)+k_{\beta 1}(z)+k_{\beta}(z))C_{R(m)}(z) \\ &- k_{\mathrm{trs}}(z)C_S(z)C_{R(m)}(z) - k_{\mathrm{trm}}(z)C_M(z)C_{R(m)}(z) \\ &+ k_{\mathrm{mi}}(z)C_M(z)^3(\delta_{m,1}+\delta_{m,2}) - f_{\mathrm{o}}k_{\mathrm{o}}(z)C_{O_2}(z)^{1.1}\,C_{R(m)}(z) \\ &- k_{\mathrm{trp}}(z)\mu_1(z)C_{R(m)}(z) \\ &+ k_{\mathrm{trp}}(z)\lambda_0(z)m\,C_{P(m)}(z)(1-\delta_{m,0}-\delta_{m,1}) \\ m &= 0,\ldots,\infty \end{aligned} \tag{A.2}$$

Eqs. (A.1) and (A.2) can be transformed into the pgf domain using the pgf Transform Table developed by the authors Asteasuain (2003), Asteasuain, Sarmoria, et al. (2002), avoiding an otherwise tedious and time consuming procedure. The resulting equations for the pgf transforms of the polymer and radical MWDs are

pgf of the polymer MWD ($a = 0, 1, 2$)

$$\begin{aligned}\frac{\mathrm{d}(\hat{\varphi}_{a,l}(z)v(z))}{\mathrm{d}z} &= \frac{1}{2}k_{\mathrm{tc}}(z)\sum_{j=0}^{a}\binom{a}{j}\hat{\phi}_{j,l}(z)\hat{\phi}_{a-j,l}(z) + (k_{\mathrm{tdt}}(z)+k_{\beta 1}(z) \\ &+ k_{\beta}(z))\hat{\phi}_{a,l}(z) + k_{\mathrm{trs}}(z)C_S(z)\hat{\phi}_{a,l}(z) + k_{\mathrm{trp}}(z)\mu_1(z)\hat{\phi}_{a,l}(z) \\ &- k_{\mathrm{trp}}(z)\lambda_0(z)\hat{\varphi}_{a+1,l}(z) + k_{\mathrm{trm}}(z)C_M(z)\hat{\phi}_{a,l}(z) \end{aligned} \tag{A.3}$$

where

$$\hat{\varphi}_{a,l}(z) = \varphi_{a,l}(z)\mu_a(z) \tag{A.4}$$

$$\hat{\phi}_{a,l}(z) = \phi_{a,l}(z)\lambda_a(z) \tag{A.5}$$

pgf of the radical MWD ($a = 0, 1, 2$)

$$\begin{aligned}\frac{\mathrm{d}(\hat{\phi}_{a,l}(z)v(z))}{\mathrm{d}z} &= k_{\mathrm{o}}(z)C_{O_2}(z)^{1.1}\,C_M(z)\delta_{a,0} + 2f_{I_1}k_{I_1}(z)C_{I_1}(z)\delta_{a,0} \\ &+ 2f_{I_2}k_{I_2}(z)C_{I_2}(z)\delta_{a,0} + k_{\mathrm{p}}(z)C_M(z)l\sum_{j=0}^{a}\binom{a}{j}\hat{\phi}_{j,l}(z) \\ &- k_{\mathrm{p}}(z)C_M(z)\hat{\phi}_{a,l}(z) + (k_{\mathrm{tdt}}(z)+k_{\beta 1}(z)+k_{\beta}(z))\lambda_0(z)\delta_{a,0} \\ &+ k_{\mathrm{trs}}(z)C_S(z)\lambda_0(z)\delta_{a,0} + k_{\mathrm{trm}}(z)C_M(z)\lambda_0(z)l \\ &- k_{\mathrm{tc}}(z)\lambda_0(z)\hat{\phi}_{a,l}(z) - (k_{\mathrm{tdt}}(z)+k_{\beta 1}(z)+k_{\beta}(z))\hat{\phi}_{a,l}(z) \\ &- k_{\mathrm{trs}}(z)C_S(z)\hat{\phi}_{a,l}(z) - k_{\mathrm{trm}}(z)C_M(z)\hat{\phi}_{a,l}(z) \\ &+ k_{\mathrm{mi}}(z)C_M(z)^3(l+2^a l^2) - f_{\mathrm{o}}k_{\mathrm{o}}(z)C_{O_2}(z)^{1.1}\,\hat{\phi}_{a,l}(z) \\ &- k_{\mathrm{trp}}(z)\mu_1(z)\hat{\phi}_{a,l}(z) + k_{\mathrm{trp}}(z)\lambda_0(z)\hat{\varphi}_{a+1,l}(z) \end{aligned} \tag{A.6}$$

A closure technique is employed to express $\hat{\varphi}_{3,l}(z)$ (appearing in Eqs. (A.5) and (A.6) when $a = 2$) as function of $\hat{\varphi}_{0,l}(z)$, $\hat{\varphi}_{1,l}(z)$ and $\hat{\varphi}_{2,l}(z)$ (Asteasuain, 2003)

$$\hat{\varphi}_{3,l}(z) = \frac{\hat{\varphi}_{2,l}(z)^2}{\hat{\varphi}_{1,l}(z)} + \hat{\varphi}_{2,l}(z) - \hat{\varphi}_{1,l}(z) \tag{A.7}$$

Eqs. (A.3)–(A.6) must be solved for different values of the dummy variable l as required by the inversion methods.

Balance equations for the a th order moments of the polymer and radical MWDs are also obtained from Eqs. (A.1) and (A.2) using well-established techniques (Katz & Saidel, 1967).

a-th order moment of the polymer MWD ($a = 0, 1, 2$)

$$\begin{aligned}\frac{\mathrm{d}(\mu_a(z)v(z))}{\mathrm{d}z} &= \frac{1}{2}k_{\mathrm{tc}}(z)\sum_{j=0}^{a}\binom{a}{j}\lambda_j(z)\lambda_{a-j}(z) + (k_{\mathrm{tdt}}(z)+k_{\beta 1}(z) \\ &+ k_{\beta}(z))\lambda_a(z) + k_{\mathrm{trs}}(z)C_S(z)\lambda_a(z) + k_{\mathrm{trp}}(z)\mu_1(z)\lambda_a(z) \\ &- k_{\mathrm{trp}}(z)\lambda_0(z)\mu_{a+1}(z) + k_{\mathrm{trm}}(z)C_M(z)\lambda_a(z) \end{aligned} \tag{A.8}$$

a-th order moment of the radical MWD ($a = 0, 1, 2$)

$$\begin{aligned}\frac{\mathrm{d}(\lambda_a(z)v(z))}{\mathrm{d}z} &= k_{\mathrm{o}}(z)C_{O_2}(z)^{1.1}\,C_M(z)\delta_{a,0} + 2f_{I_1}k_{I_1}(z)C_{I_1}(z)\delta_{a,0} \\ &+ 2f_{I_2}k_{I_2}(z)C_{I_2}(z)\delta_{a,0} + k_{\mathrm{p}}(z)C_M(z)\sum_{j=0}^{a}\binom{a}{j}\lambda_j(z) \\ &- k_{\mathrm{p}}(z)C_M(z)\lambda_a(z) + (k_{\mathrm{tdt}}(z)+k_{\beta 1}(z)+k_{\beta}(z))\lambda_0(z)\delta_{a,0} \\ &+ k_{\mathrm{trs}}(z)C_S(z)\lambda_0(z)\delta_{a,0} + k_{\mathrm{trm}}(z)C_M(z)\lambda_0(z) \\ &- k_{\mathrm{tc}}(z)\lambda_0(z)\lambda_a(z) - (k_{\mathrm{tdt}}(z)+k_{\beta 1}(z)+k_{\beta}(z))\lambda_a(z) \\ &- k_{\mathrm{trs}}(z)C_S(z)\lambda_a(z) - k_{\mathrm{trm}}(z)C_M(z)\lambda_a(z) \\ &+ k_{\mathrm{mi}}(z)C_M(z)^3(1+2^a) - f_{\mathrm{o}}k_{\mathrm{o}}(z)C_{O_2}(z)^{1.1}\,\lambda_a(z) \\ &- k_{\mathrm{trp}}(z)\mu_1(z)\lambda_a(z) + k_{\mathrm{trp}}(z)\lambda_0(z)\mu_{a+1}(z) \end{aligned} \tag{A.9}$$

The third-order moment of the polymer MWD, appearing in Eqs. (A.8) and (A.9) when $a = 2$, is expressed as function of the lower order moments assuming a log-normal distribution (Brandolin et al., 1996).

$$\mu_3 = \left(\frac{\mu_2}{\mu_1}\right)^3\mu_0 \tag{A.10}$$

References

Asteasuain, M. (2003). *Modelado de procesos de polimerización y procesos pos-reactor. Aplicación de nuevas técnicas para la predicción de la dis-*

tribución de pesos moleculares con verificación experimental. Ph.D. Thesis. Argentina: Universidad Nacional del Sur, Bahía Blanca.

Asteasuain, M., & Brandolin, A. (2006). Optimal operation of ethylene polymerization reactors for tailored MWD. In *International Symposium on Advanced Control of Chemical Processes* (pp. 235–240).

Asteasuain, M., Brandolin, A., & Sarmoria, C. (2002). Recovery of molecular weight distributions from transformed domains. Part II: Application of numerical inversion methods. *Polymer*, *43*, 2529–2541.

Asteasuain, M., Pereda, S., Lacunza, M. H., Ugrin, P. E., & Brandolin, A. (2001). Industrial high pressure ethylene polymerization initiated by peroxide mixtures: A reduced mathematical model for parameter adjustment. *Polymer Engineering and Science*, *41*, 711–726.

Asteasuain, M., Sarmoria, C., & Brandolin, A. (2002). Recovery of molecular weight distributions from transformed domains. Part I: Application of pgf to mass balances describing reactions involving free radicals. *Polymer*, *43*, 2513–2527.

Asteasuain, M., Ugrin, P. E., Lacunza, M. H., & Brandolin, A. (2001). Effect of multiple feedings in the operation of a high-pressure polymerization reactor for ethylene polymerization. *Polymer Reaction Engineering*, *9*, 163–182.

Brandolin, A., Asteasuain, M., Sarmoria, C., López-Rodríguez, A., Whiteley, K. S., & del Amo Fernández, B. (2001). Numerical inversion techniques in the recovery of molecular weight distribution expressed in different transformed domains. Experimental validation. *Polymer Engineering and Science*, *41*, 1156–1170.

Brandolin, A., Lacunza, M. H., Ugrin, P. E., & Capiati, N. J. (1996). High pressure polymerization of ethylene. An improved mathematical model for industrial tubular reactors. *Polymer Reaction Engineering*, *4*, 193–291.

Katz, S., & Saidel, G. M. (1967). Moments of the size distribution in radical polymerization. *AIChE Journal*, *13*, 319–325.

Kim, D., & Iedema, P. D. (2004). Molecular weight distribution in low-density polyethylene polymerization; impact of scission mechanisms in the case of a tubular reactor. *Chemical Engineering Science*, *59*, 2039–2052.

Kiparissides, C., Verros, G., Kalfas, G., Koutoudi, M., & Kantzia, C. (1993). A comprehensive mathematical model for a multizone tubular high-pressure LDPE reactor. *Chemical Engineering Communications*, *121*, 193–217.

Kiparissides, C., Verros, G., & Pertsinidis, A. (1994). On-line optimization of a high-pressure low-density polyethylene tubular reactor. *Chemical Engineering Science*, *49*, 5011–5024.

Lacunza, M. H., Ugrin, P. E., Brandolin, A., & Capiati, N. J. (1998). Heat transfer coefficient in a high pressure tubular reactor for ethylene polymerization. *Polymer Engineering and Science*, *38*, 992–1013.

Mavridis, H., & Kiparissides, C. (1985). Optimization of a high-pressure polyethylene reactor. *Polymer Processing Engineering*, *3*, 263–290.

Pladis, P., & Kiparissides, C. (1998). A comprehensive model for the calculation of molecular weight-long-chain branching distribution in free-radical polymerizations. *Chemical Engineering Science*, *53*, 3315–3333.

Process Systems Enterprise, Ltd. (2005). *gPROMS introductory user guide*.

Schmidt, C., Busch, M., Lilge, D., & Wulkow, M. (2005). Detailed molecular structure modeling—A path forward to designing application properties of ldPE. *Macromolecular Materials and Engineering*, *290*, 404–414.

Wells, G. J., & Ray, W. H. (2005). Prediction of polymer properties in LDPE reactors. *Macromolecular Materials and Engineering*, *290*, 319–346.

Zabisky, R. C., Chan, W. M., Gloor, P. E., & Hamielec, A. E. (1992). A kinetic model for olefin polymerization in high-pressure tubular reactors: A review and update. *Polymer*, *33*, 2243–2262.